Adsorption and diffusion of hydrogen in Zircaloy-4

Elodie Torres, Jean Desquines, Marie-Christine Baietto, Michel Coret, Franz Wehling, Martine Blat-Trieix, Antoine Ambard

Adsorption and diffusion of hydrogen in Zircaloy-4

Torres É.[1*], Desquines J.[1], Baietto M.C.[2], Coret M.[3], Wehling F.[4], Blat-Yrieix M.[5], Ambard A.[5]

[1]Institut de Radioprotection et de Sûreté Nucléaire (IRSN), Centre d'Etudes de Cadarache, PSN-RES/SEREX/LE2M, BP3, F-13115 Saint-Paul lez Durance Cedex (France)
[2]Laboratoire de Mécanique des Contacts et des Structures (LaMCoS), INSA de Lyon, UMR 5259, 69621 Villeurbanne cedex, (France)
[3]École Centrale de Nantes, Institut de recherche en génie civil et mécanique (GEM), UMR 6183, 44321 Nantes, (France)
[4]École Centrale de Paris, laboratoire LPE, 92295 Chatenay Malabry Cedex (France)
[5]EDF-R&D, Les Renardières, département MMC, 77818 Moret sur Loing, (France)
*elodie.torres@irsn.fr

Abstract. Hydrogen in zirconium alloys is considered in many nuclear safety issues. Below 500°C, rather limited knowledge is available on the combined hydrogen adsorption at the sample surface and diffusion in the metal. A modeling of hydrogen gaseous charging has been established starting with a set of relevant laws and parameters derived from open literature. Simulating the hydrogen charging process requires simultaneous analysis of gaseous surface adsorption, hydrogen solid-solution diffusion and precipitation, when exceeding the material solubility limit. The modeling has been extended to reproduce the solid-gas exchange. Gaseous charging experiments have been performed at 420°C on Stress Relieved Annealed (SRA) Zircaloy-4 cladding samples to validate the model. The sample hydrogen content has been systematically measured after charging and compared to the calculated value thus providing a validation of the adsorption modeling. Complementary tests have been carried out on Recrystallized Annealed (RXA) Zircaloy-4 rods to characterize the combined diffusion and adsorption process. The hydrogen concentration distribution has been characterized using an inverse technique based on destructive analyses of the samples. This additional set of data was relevant for the validation of the hydrogen combined adsorption/diffusion modeling up to 420°C.

KEYWORDS: Zircaloy-4, Hydrogen, diffusion, precipitation, modeling

Introduction

Under normal operation in nuclear reactors, zirconium based cladding alloys are affected by water corrosion and hydrogen pick-up according to Equation 1.

$$Zr + 2H_2O \longrightarrow ZrO_2 + 2H_2 \qquad \text{(Eq. 1)}$$

Depending on the corrosion temperature, the dissolved hydrogen can precipitate when exceeding the material solubility limit. In pile, the migration of hydrogen induced by thermal gradient in the cladding radial direction promotes accumulation of hydrides at the cladding outer diameter. After several years irradiation, a hydride rich rim is formed as illustrated in Figure 1.

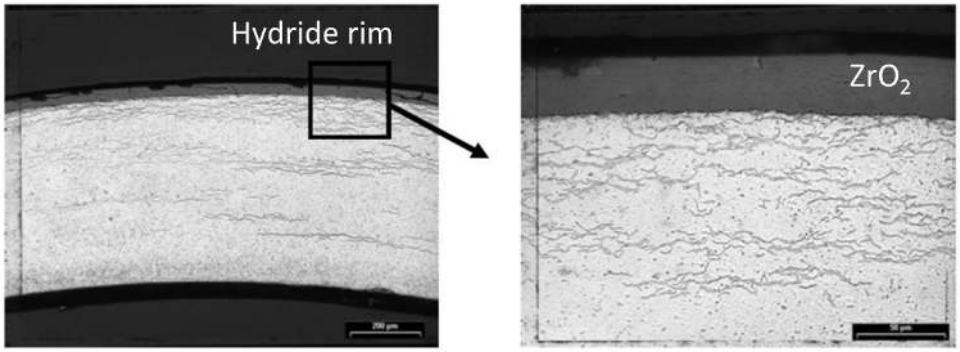

Figure 1: Cladding microstructure in PWR normal operating condition [1]

Hydrogen has to be considered in many safety issues. Indeed, it changes many properties of zirconium alloys such as their mechanical or metallurgical behaviors. Hydrogen charged specimens are formed in laboratories to investigate part of the behavior of the irradiated material. Two main hydrogen charging techniques are used: cathodic charging at room temperature and gaseous charging at a temperature close to irradiation conditions. Considering this second charging technique, rather few studies address the hydrogen adsorption and diffusion in the metal. In this work we intend to provide a modeling of the gaseous charging of zirconium specimen as well as an experimental validation.

Modeling

Markowitz experiments evidenced that hydrogen diffuses towards the colder regions [2] showing that a driving force for solid solution diffusion is temperature gradient. The diffusion is also driven by concentration gradient and to a lower extent by stress gradient as shown by Marino and Kammenzind [3-5]. In the following, the modeling of thermal diffusion only neglects the stress gradient influence as suggested by Kammenzind [5].

The total hydrogen content (C_T) is thus considered to be the sum of two components, the precipitated hydrogen content (C_p) and the dissolved hydrogen content in the α-phase (C_d) according to Eq. 2, with the concentrations expressed in weight particles per million (wppm).

$$\mathrm{C} = \mathrm{C_p} + \mathrm{C_d} \quad \text{(Eq. 2)}$$

During thermal diffusion, under time-increasing total hydrogen content, the dissolved hydrogen concentration is limited, assuming equilibrium conditions, by the hydrogen Terminal Solid Solubility for Precipitation (TSSP), C_{TSSP}. During this precipitation phase, the dissolved hydrogen content in the α-phase remains close, but not systematically equal, to the C_{TSSP} limit [6]. As a simple summary, during precipitation (Eq. 3), the solid-solution content is associated to equation 4.

$$\frac{\mathrm{dC_p}}{dt} > 0 \quad \text{(Eq. 3)}$$

$$\mathrm{C_d} = C_{sp} + C_{supercharging} \quad \text{(Eq. 4)}$$

$C_{supercharging}$ corresponds to a few wppm dissolved hydrogen excess compared to the TSSP. This excess was evidenced by Marino [7] and is usually called “hydrogen supercharging”.

The hydride precipitation kinetics is rather slow [8-9] and is assumed to be proportional to the level of supercharging as proposed by Marino and Kammenzind [5;7]. This hydride precipitation kinetics is described in equation 5, where <X> is the positive value of X.

$$\frac{\partial C_p}{\partial t} = \alpha^2 \langle C_d - C_{sp} \rangle \quad \text{(Eq. 5)}$$

The proportionality coefficient is given by equation 6 [6],

$$\alpha = 306{,}6\, exp^{-\frac{5880}{T}} \quad \text{(Eq. 6)}$$

where α is a parameter related to the hydride precipitation kinetics in $s^{-1/2}$, and T is the temperature in Kelvin.

During heating, the local hydrogen content is governed by hydride dissolution. Under such conditions, the dissolved hydrogen content is limited by the Terminal Solid Solubility for Dissolution (TSSD). Additionally, the dissolution kinetics is a fast process. During this phase, the dissolved hydrogen content is simply assessed by a maximum value being equal to C_{TSSD}. The dissolution phase is defined by equation 7 and 8.

$$\mathrm{C_p} > 0 \text{ and } \frac{\mathrm{dC_p}}{dt} < 0 \quad \text{(Eq. 7)}$$

$$\mathrm{C_d} = C_{TSSD} \quad \text{(Eq. 8)}$$

At a given temperature, the C_{TSSD} value is significantly higher than C_{TSSP} [10-13]. The dissolution and precipitation solubility limits are given by equations 9 and 10. TSSD is frequently considered as the solubility limit at equilibrium [14]. However, there is some controversy on this point.

$$C_{TSSD}(wppm) = 9{,}9.10^4\ exp^{-\frac{4162}{T(K)}} \quad \text{(Eq. 9)}$$

$$C_{TSSP}(wppm) = 6{,}91.10^4\ exp^{-\frac{3596}{T(K)}} \quad \text{(Eq. 10)}$$

The hydrogen diffusion within hydrides is slow and neglected [15]. The local hydride fraction is considered as negligible in order to simplify the diffusion equation. The hydrogen flux, without intense hydrostatic stress, derives from equation 11,

$$\vec{J} = -D\left(\vec{\nabla}C_d + \frac{Q^* C_d}{RT^2}\vec{\nabla}T\right) \quad \text{(Eq. 11)}$$

where J is the hydrogen flux (mm/s), Q* is the heat of transport, equal to 24000 J/mol [16-17], T is the absolute temperature (Kelvin), R is the gas constant (J/mol/K) and D is the diffusion coefficient of hydrogen in the α-phase (mm^2/s). D can be described from an Arrhenius law according to equation 12 [18].

$$D = 0.79\ exp^{-\frac{5058}{T}}\ \text{in mm}^2\text{/s} \quad \text{(Eq. 12)}$$

In the presence of precipitated hydrides, the α-phase diffusion is described by equations 13 and 14.

$$\frac{\partial C_d}{\partial t} = -\vec{\nabla}\vec{\mathrm{J}} - \alpha^2\langle C_d - C_{sp}\rangle \quad \text{(Eq. 13)}$$

$$\frac{\partial C_T}{\partial t} = \vec{\nabla}\vec{\mathrm{J}} \quad \text{(Eq. 14)}$$

The literature was intensively analyzed in order to identify reference experiments for code validation [16-17;19-21] considering thermal diffusion only.

The modeling has been extended to account for solid-gas exchange. In the literature, it has been essentially addressed at elevated temperature. The hydrogen concentration in metal versus gaseous pressure at equilibrium was experimentally evidenced to follow a Sievert law [22-23] described in equation 15,

$$C_d = kp^{1/2}exp\left(-\frac{Q}{RT}\right) \quad \text{(Eq. 15)}$$

where k is a kinetic constant, p is the gaseous pressure and Q is the activation energy in the α-phase region.

The modeling relies on an explicit 1D integration scheme of diffusion equations in axisymmetric or cartesians coordinates. The model provides hydrogen radial concentration profile after any simulated exposure at elevated temperature. To model the solid/gas exchanges two possible assumptions are considered: a constant interface concentration (Eq 15 like conditions) or a constant absorbed flux depending on the environment gas pressure p as described by equation 16,

$$\frac{\partial C_d}{\partial t} = k.p_{H_2}^n \quad \text{(Eq. 16)}$$

where k is a kinetic constant.

Let's consider a thin plate of thickness, e, to clarify the meaning of this boundary condition. Solid/gas exchange at both faces of this plate following Equation 16 type boundary conditions and isothermal hydrogen charging are considered.

Solving diffusion equations provides a very simplified assessment of the diffusion behavior in such component. The average hydrogen concentration in the sample (C_T) is given by time integration of equation 17.

$$\frac{dC_T}{dt} = \frac{2kD}{e} . p_{H_2}^n \quad \text{(Eq. 17)}$$

In other words, at a given gaseous pressure, there is a constant increase rate of average hydrogen content in the sample. This kind of boundary condition can lead to unlimited hydrogen adsorption, whereas equation 15 type leads to equilibrium between hydrogen content and gaseous pressure.

To qualify the modeling, several gaseous charging experiments have been performed on SRA Zircaloy-4 cladding samples. In order to provide fully coupled experiments involving hydrogen motion in metal and surface exchange, complementary tests have been carried out using plain rod RXA samples.

Materials and methods

1- Materials

The specimens investigated in this study have been cut from low tin 17x17 SRA Zircaloy-4 fuel cladding tubes and RXA rods provided by AREVA-NP. The tube specimens are 70 mm long, 9.5 mm outer diameter and 570 µm thick respectively. Oversized grains located at the outer and/or inner diameter have been observed on as-received rod samples. Consequently, rods have been spark machined from 9,8 to 7 mm of outer diameter to remove the large grains zone. Chemical composition of these samples is detailed in Table 1.

Sn (wt%)	Fe (wt%)	Cr (wt%)	O (wt%)	H (wppm)
1.3	0.21	0.10	0.13	10

Table 1: Chemical composition of the Zy-4 samples used for the hydrogen gaseous charging

2- Hydrogen Gaseous charging

The hydrogen gaseous charging is performed at the École Centrale de Paris. Each Zircaloy-4 sample is inserted in a quartz tube under vacuum. The sample is then heated by a furnace at 420°C. Once the target temperature is reached, pure hydrogen is injected into the quartz tube. Indeed, the injected pressure is linked to the target hydrogen content. The charging temperature is chosen sufficiently low to avoid cladding recristallisation and sufficiently high for allowing charging high hydrogen concentrations in a reasonable time. The charging can be performed in several hydrogen injection steps depending on the desired final concentration. The sample is then cooled down without applied stresses at 20°C/h to obtain large and representative of as-irradiated circumferential hydrides (Figure 2). The hydrogen pressure decrease in the charging device provides a direct measurement of the average hydrogen content absorbed within the sample. The maximal allowable hydrogen concentration increase in the specimen is directly related to the initial pressure in the furnace.

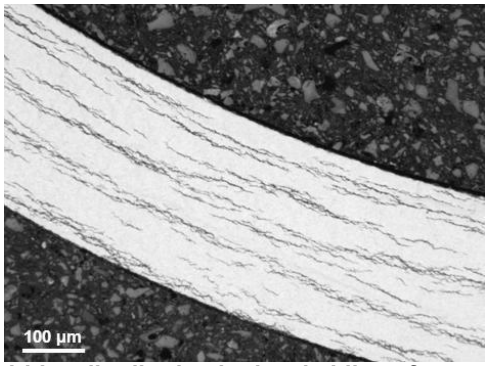

Figure 2: Example of hydrides distribution in the cladding after gaseous charging at 420°C

3- Experiment

To describe only surface/gas exchange, gaseous charging experiments have been performed on SRA Zircaloy-4 cladding tubes. Due to the thin geometry of tubes, the hydrogen is close to uniformly distributed and the surface exposed to gaseous hydrogen is large, permitting an accurate measurement of adsorption kinetics.

RXA Zircaloy-4 rods have been also used to perform radial diffusion experiments. After gaseous charging, the cylindrical sample is first machined to obtain a cone and the outer volume is then truncated into many 1 mm long crowns with inner diameter depending on its axial location after sample machining (Figure 3). The hydrogen is measured on each crown sample which is allowed to determine radial hydrogen concentration assuming axial homogeneity. These complementary tests have been performed to provide fully coupled experiments involving hydrogen diffusion and surface/gas exchange.

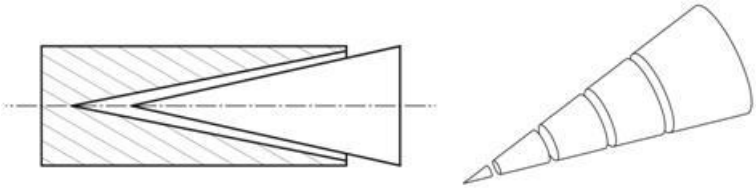

Figure 3 : Conical machining and cutting after gaseous charging of the samples

4- Hydrogen content measurement

The hydrogen content of the samples is measured after gaseous charging using a Brücker ONH mat 286 by melting the sample at 1500°C in the presence of a carrier gas (argon). After calibration, the hydrogen content is obtained by comparing the conductivity of the mixture with the one of pure argon. For tube samples, four axial locations are systematically investigated. A minimum of four analyses for each area are performed to characterize the homogeneity of hydrogen content at each location. This method provides a measurement of the average hydrogen content and the radial hydrogen profile cannot be directly measured.

Results and discussion

1- Hydrogen diffusion in a thermal gradient

The experimental data of Sawatzky and Markowitz [16;17] have first been considered for the validation of the diffusion modeling. The Sawatzky experiments have been performed on Zircaloy-2 cylindrical samples. The first test (called A) consisted in keeping during 34 days a linearly varying temperature of 130°C and 477°C at each ends of a 24 mm long sample containing initially 130 wppm hydrogen homogeneously distributed. In the second test (called B), a linearly varying temperature between 157°C and 454°C along the sample is kept during 41 days using a 24 mm long the sample containing initially 64 wppm hydrogen homogeneously distributed. The Markowitz experiments have also been performed on Zircaloy-2 cylindrical samples. In the first test, a thermal gradient of 73°C/cm during 30 days has been applied on the sample containing initially 300 wppm hydrogen homogeneously distributed. In the second test, a thermal gradient of 75°C/cm has been kept during 41.5 days on a sample containing initially 3360 wppm hydrogen uniformly distributed.
Figure 4 compares the two test results of Markowitz with calculations and Figure 5 presents the Sawatzky results compared to simulations.

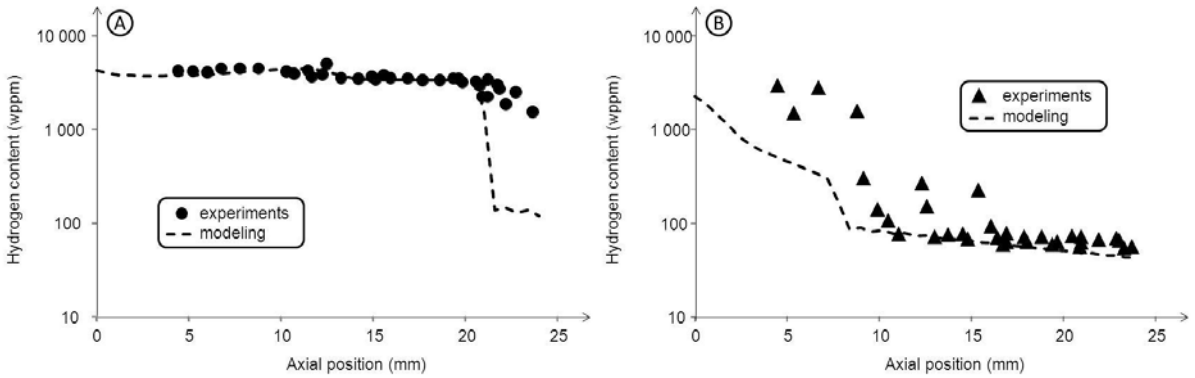

Figure 4: Hydrogen distribution in Markowitz samples [17]
(A) 41.5 days anneal
(B) 30 days anneal

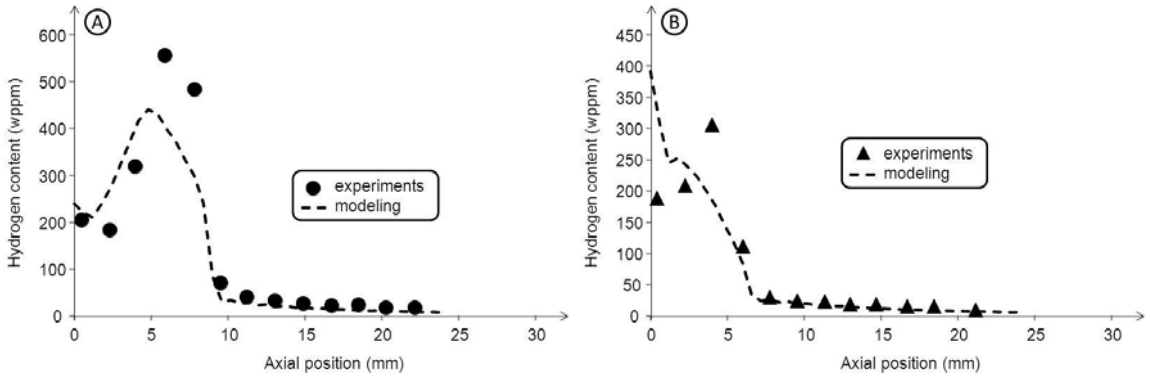

Figure 5: Hydrogen distribution in Sawatzky samples [16]
(A) 34 days anneal
(B) 41 days anneal

A good agreement is obtained between experiments and simulation. There are, however, some discrepancies, mainly identified at the end of the samples. The two-phase, α/α+δ hydride transition is acceptably simulated. However, in Markowitz first test (Figure 4A), this experimental transition is not as clear as in the simulation. Indeed, for high concentrations, hydride volume fraction should be taken into account. Actually, hydrogen diffusion within hydride is about three times slower than in the metal [15].

2- Surface/gas exchange

The present modeling has been compared to the experimental data of many samples charged by gaseous method. The experimental average hydrogen content within the sample is deduced from the hydrogen gaseous pressure decrease in the charging device. An example, where the charging has been performed in several hydrogen injection steps, is presented in Figure 6.

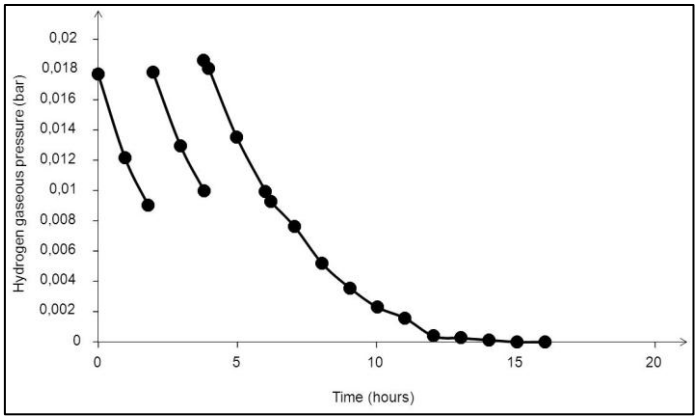

Figure 6 : Evolution of hydrogen gaseous pressure versus time at 420°C of a sample charged at 500 wppm in 3 steps with an injection hydrogen pressure around 18 mbar

First we can check that pressure decrease is really due to hydrogen absorption. The maximal allowable hydrogen concentration increase in the specimen is directly related to the initial pressure in the furnace by Equation 18,

$$p_{H_2}^{max} = m_{sample} . \frac{\Delta C_{max}^{i}}{10^6} . \frac{RT}{2V_0 M_H} \qquad \text{(Eq. 18)}$$

where $p_{H_2}^{max}$ is the initial hydrogen pressure of the current injection step (bar), m_{sample} is the weight of the sample (g), ΔC_{max}^{i} is the maximal hydrogen concentration increase at each injection step i (wppm), V_0 is the hydrogen gas volume in the device, R is the gas constant (J/mol/K), T is the hydrogen charging temperature (Kelvin) and M_H is the hydrogen molecular weight (1 g/mol).

Let ΔC_i be the hydrogen content variation at each step (wppm) defined by equation 19,

$$\Delta C_i = \frac{\Delta p}{p_{H_2}^{max,i}} \qquad \text{(Eq. 19)}$$

where $p_{H_2}^{max}$ is the initial hydrogen pressure and Δp is the decrease in hydrogen pressure during absorption. The total average hydrogen content in the sample (ΔC_T) is thus expressed by equation 20. In this equation, C_0 is the hydrogen content in the as received material.

$$\Delta C_T = \sum \Delta C_i + C_o \quad \text{(Eq. 20)}$$

The average hydrogen concentration of the studied tubes was approximately 100, 200, 400 and 500 wppm. The average hydrogen content calculated in the sample using eq. 15 for gas absorption can be compared to the measurements. The main results are summarized in Table 2. The good consistency between experimentally measured hydrogen content and the calculated one from pressure decrease shows that pressure can be used to measure the sample hydrogen content.

samples	Hydrogen content (ppm)		
	target	experimental	predicted
H55	500	442	505
H58	200	157	187
H65	400	337	349
H67	100	93	103

Table 2: Hydrogen contents after gaseous charging versus code predictions

Whereas hydrogen adsorption is clearly governed by a Sievert law at elevated temperature [22;23], the hydrogen charging experiments can lead to the absorption of the whole gaseous content of the furnace as illustrated in Figure 6. This trend is not compatible with Sievert like boundary conditions (Eq. 15) but with constant adsorption flux (Eq. 16 like condition). Analysis of the hydrogen absorption kinetics allows us to determine the pressure exponent of Eq. 16.
Hydrogen absorption kinetics can be fitted to a “Langmuir” type law [24;25]. The rate of average hydrogen content in the sample follows equation 21.

$$\frac{\mathrm{dC_T}}{\mathrm{dt}} = \mathrm{A}\frac{\mu.\mathrm{p_{H_2}}}{1+\mu.\mathrm{p_{H_2}}} \quad \text{(Eq. 21)}$$

where A is a kinetics constant and μ is a term proportional to $\frac{2kD}{e}$.

The adsorption rate is proportional to $\mathrm{p_{H_2}}$, this means that the rate limiting phenomenon is the H_2 molecule adsorption at the sample surface rather than H_2 dissociation [25].

Considering that in our experiments $\mu.\mathrm{p_{H_2}} \ll 1$, the combination of Eq. 17 and Eq. 21 results in Eq. 22,

$$A * \mu = \frac{2kD}{e} \quad \text{(Eq. 22)}$$

where A*μ is in $\frac{wppm}{s.bar}$, k in $\frac{wppm}{mm.bar}$, e in mm and D in mm^2/s.

In the case of tube-type specimens and low hydrogen pressure, the solid/gas exchange is therefore described by Eq. 23,

$$\boxed{\frac{dC_d}{dx} = 658.\mathrm{p_{H_2}}} \quad \text{(Eq. 23)}$$

where $\frac{dC_d}{dx}$ is in $\frac{wppm}{mm}$ and p in bar.

The agreement between experiment and theory is rather good as illustrated in Figure 7 in the whole range of hydrogen contents and charging conditions. The weight gain $\frac{1}{\mathrm{S}}\frac{\mathrm{d\Delta m}}{\mathrm{dt}}$ ($g/cm^2.s$) is also used to characterize the hydrogen gaseous charging kinetics.

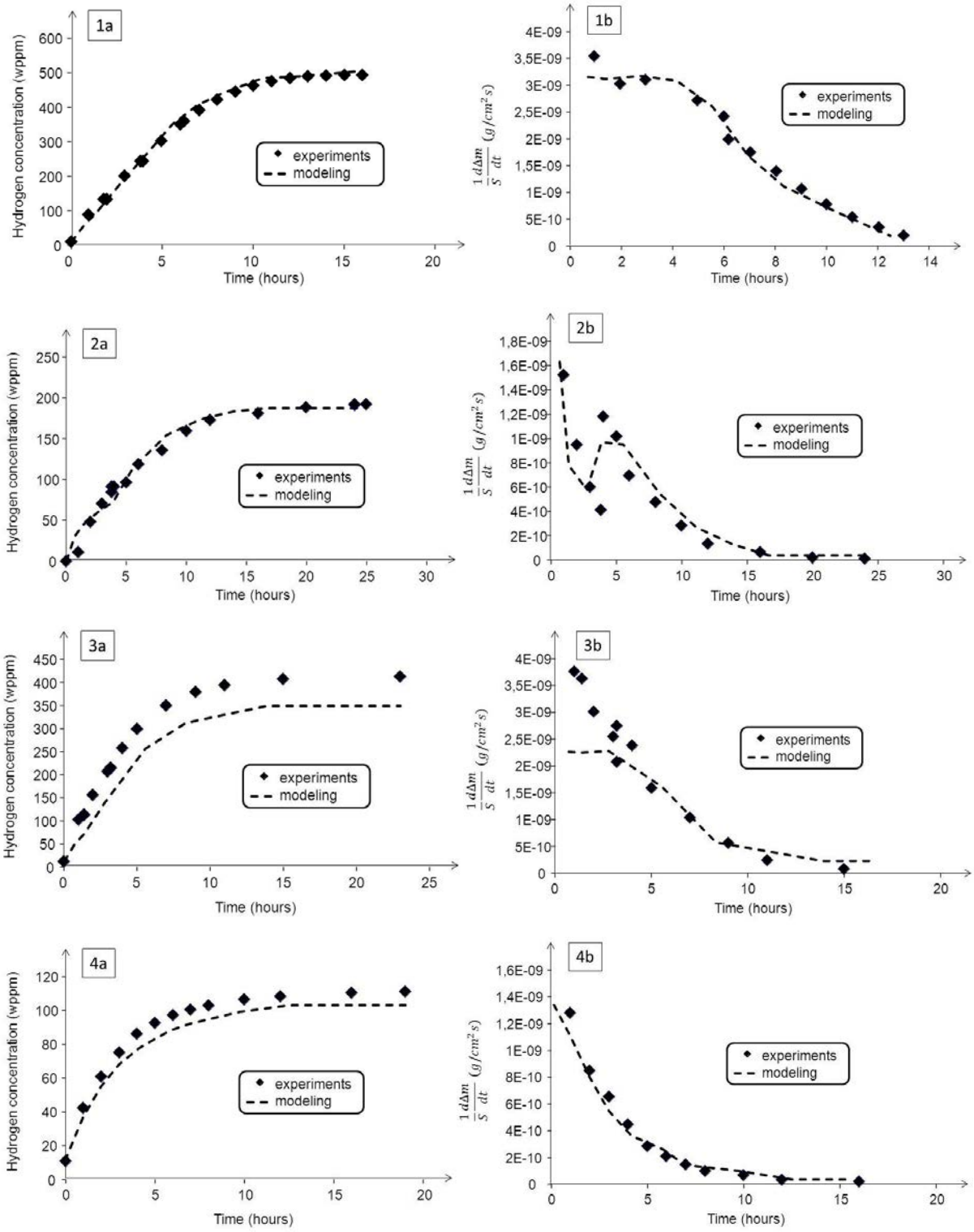

Figure 7 : Hydrogen charging experiments of 8 different tubes at 420°C: experiments versus modeling
(A) hydrogen content evolution in the sample
(B) hydrogen charging kinetics

The modeling provides assistance to laboratory gaseous charging experiments. The expected hydrogen profile and sample average contents can be anticipated from calculation. The modeling leads to a homogeneous distribution of the hydrogen which is consistent with the metallographic examinations (Figure 8).

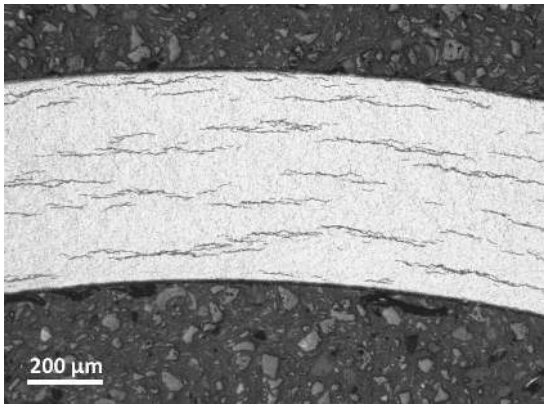

Figure 8: Distribution of hydrides in a Zircaloy-4 tubes after gaseous charging with 100 wppm of hydrogen

3- Combined hydrogen diffusion and Surface/gas exchange

Complementary tests on RXA Zircaloy-4 rods have been performed to provide fully coupled experiments involving hydrogen distribution and surface/gas exchange. The radial profile of hydrogen content derived from measurements and the one derived from simulations are illustrated in Figure 9. An inverse technique based on destructive characterization of the sample has been used to deduce the hydrogen profile. This technique consists in postulating a hydrogen distribution and adjusting its shape to find average hydrogen content as close as possible to measurements on crown pellets machined on the rod sample (Figure 3). The hydrogen concentration varies between 60 wppm at the center of the rod up to 100 wppm at the outer diameter. For the simulations, the solid/gas exchange coefficient and/or the diffusion coefficient was adjusted to reproduce as closely as possible the experiment. The diffusion coefficient is potentially influenced by material texture and the charging kinetics appears to be faster than for tubes and some differences grain size and microstructure could also affect both, diffusion coefficient and solid/gas exchange. Kearns mentions that the diffusion coefficient in the c-axis direction of hcp Zircaloy-4 is about two times larger than in the a-direction. This would imply a lower diffusion coefficient to accurately simulate rods [18].

The measured hydrogen profile is acceptably reproduced by simulation. A sensitivity study to diffusion coefficient and adoption kinetics was done by adjusting the D_0 and k parameters in Eq. 24 and Eq. 25. It was not possible to find parameters leading to the measured profile in the entire range of radii. However two extreme sets of values are identified, the first one fitting the distribution at the center of the cylindrical sample and the second describing accurately the distribution at the outer diameter of the sample as illustrated in Figure 9. The results are different but remain consistent with the expected values obtained for tubes (Eq.12 and Eq. 23).

$$D = D_0 \, exp\left(-\frac{5058}{T}\right) \qquad \text{(Eq. 24)}$$

$$\frac{dC_d}{dx} = k.p_{H2} \qquad \text{(Eq. 25)}$$

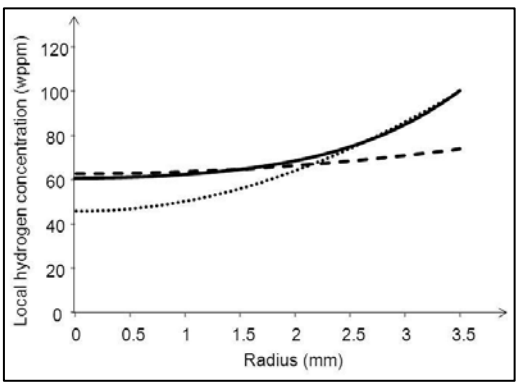

Figure 9: Hydrogen distribution within the sample: measurements versus modeling

Conclusion

In this study, a quantitative modeling of hydrogen gaseous charging of Zircaloy-4 samples is proposed taking into account both the solid/gas exchange and the thermal diffusion of hydrogen in the metal.

Some gaseous charging experiments at 420°C of thin Zircaloy-4 fuel cladding tubes have been interpreted assuming a hydrogen flux at the solid/gas interface proportional to the hydrogen pressure. The modeling is consistent with measurements and can now be used to monitor hydrogen charging experiments. The expected hydrogen profile and sample average contents can be anticipated from calculations.

Experiments were designed on rod samples in order to obtain a radial hydrogen profile on RXA Zr-4 rods. The solid/gas exchange kinetics and diffusion coefficient had to be adjusted to reproduce the measured hydrogen profile in the sample. This is probably due to a strong sensitivity of the diffusion coefficients and solid/gas exchange to material microstructure.

References

1) **P Bossis**, "Comparison of the high burn-up corrosion on M5 and Low Tin Zircaloy-4", *ASTM 14th International Symposium on Zirconium in the Nuclear Industry*, Stockholm, June 13-17, (2004)
2) **JM Markowitz**, "Hydrogen redistribution in thin plates of zirconium under large thermal gradients", *Westinghouse Atomic Power Division (USA) report*, WAPD-TM-104, (1958)
3) **G.P Marino**, "A numerical calculation of the redistribution of an interstitial solute in a thermal gradient", *Nuclear Science and Engineering*, **49**, 93-98, (1972)
4) **G.P Marino**, "Hydiz a 2 dimensional computer program for migration of interstitial solutes of finite solubility in a thermal gradient", *Westinghouse Atomic Power Division (USA) report*, WAPD-TM-1157, (1974)
5) **BF Kammenzind**, "Hydrogen pickup and redistribution in alpha-annealed Zircaloy-4", *ASTM STP 1295*, 338-370, (1996)
6) **R Westerman**, "Charging Zircaloy-2 with hydrogen beyond the solubility limit", *Journal of Nuclear Materials*, **18**, 31-38, (1966)
7) **G.P Marino**, "Hydrogen supercharging in Zircaloy", *Material Science and Engineering*, **7**, 335-341, (1971)
8) **O Zanellato**, "Synchrotron diffraction study of dissolution and precipitation kinetics of hydrides in Zircaloy-4", *Journal of Nuclear Materials*, **420**, 537-547, (2012)
9) **K Une**, "Dissolution and precipitation behavior of hydrides in Zircaloy-2 and high Fe Zircaloy", *Journal of Nuclear Materials*, **322**, 66-72, (2003)
10) **WH Erickson**, "The influence of alloying elements on the terminal solubility of hydrogen in alpha-zirconium", *Journal of Nuclear Materials*, **13**, 2, 254, (1964)
11) **GH Slattery**, "The terminal solubility oh hydrogen in Zirconium alloys between 30 and 400°C", *Journal of the Institute of Metals*, **95**, 43, (1967)
12) **M Jovanovic, A Stern, H Kneis, GC Westherly, M Leger**, "Thermal diffusion of hydrogen and hydride precipitation in Zr-Nb pressure tube alloys", *Canadian Metallurgical Quarterly*, **27**, 4, 323, (1988)
13) **DO Northwood, U Kosasih, "**Hydrides and delayed hydrogen cracking in Zirconium and its alloys"**,** *International Metals Reviews*, **28**, 92-121, (1983)
14) **JJ Kearns**, "Terminal solubility and partitioning of hydrogen in the alpha phase of Zirconium, Zircaloy-2 and Zircaloy-4", *Journal of the Nuclear Materials*, **22**, 292-303, (1967)
15) **C Korn and D Goren, "***NMR study of hydrogen diffusion in zirconium hydride"***,** Physical Review B, **33**, (1), 68-78, (1986)
16) **A Sawatzky**, "Hydrogen in Zircaloy 2; its distribution and heat of transport", *Journal of Nuclear Materials*, **2**, 321, (1960)
17) **JW Markowitz**, "The thermal diffusion of hydrogen in alpha-delta Zircaloy 2", *Transactions of the Metallurgical Society of AIME*, **221**, 819, (1961)
18) **JJ Kearns**, "Diffusion coefficient of hydrogen in alpha Zirconium, Zircaloy-2 and Zircaloy-4", *Journal of Nuclear Materials*, **43**, 330-338, (1971)
19) **HS Hong**, "Thermotransport of hydrogen in Zircaloy-4 and modified Zircaloy-4", *Journal of Nuclear Materials*, **257**, 15-20, (1998)
20) **A Sasahara**, "Experiment of hydrogen migration under temperature gradient in irradiated cladding", *International topical meeting on light wator reactor fuel performance*, 532-539, Kyoto Japan, (2005)
21) **M Sugisaki**, "Estimation of hydrogen redistribution in Zircaloy cladding of spent fuel under thermal conditions of dry storage and evaluation of its influence on mechanical properties of the cladding", *TECDOC 1316*, IAEA report 63, (2002)
22) **MW Mallet and WM Albrecht**, "Low-pressure solubility and diffusion of hydrogen in zirconium", *Journal of the Electrochemical Society*, **104**, **3**, 142, (1957)
23) **EA Gulbransen**, "Solubility and decomposition pressures of hydrogen in alpha-zirconium", Transaction of AIME (*Journal of Metals)*, 136, (1955)